



HAL
open science

Heat transfer in a near-critical fluid saturated porous medium: Piston effect and viscous slowing down

Didier Lasseux, Bernard Zappoli, Samuel Marre, Yves Garrabos

► To cite this version:

Didier Lasseux, Bernard Zappoli, Samuel Marre, Yves Garrabos. Heat transfer in a near-critical fluid saturated porous medium: Piston effect and viscous slowing down. *Physical Review Fluids*, 2024, 9 (12), pp.124402. 10.1103/PhysRevFluids.9.124402 . hal-04837573

HAL Id: hal-04837573


<https://hal.science/hal-04837573v1>

Submitted on 13 Dec 2024


HAL is a multi-disciplinary open access archive for the deposit and dissemination of scientific research documents, whether they are published or not. The documents may come from teaching and research institutions in France or abroad, or from public or private research centers.

L'archive ouverte pluridisciplinaire **HAL**, est destinée au dépôt et à la diffusion de documents scientifiques de niveau recherche, publiés ou non, émanant des établissements d'enseignement et de recherche français ou étrangers, des laboratoires publics ou privés.



Heat transfer in a near-critical fluid saturated porous medium: Piston effect and viscous slowing down

Didier Lasseux ^{*}

Université de Bordeaux, CNRS, Bordeaux INP, I2M, UMR 5295, F-33400 Talence, France

Bernard Zappoli 

CNES, 18 Avenue Edouard Belin, 31000 Toulouse, France

Samuel Marre  and Yves Garrabos 

Université de Bordeaux, CNRS, Bordeaux INP, ICMCB-UMR 5026, 33600 Pessac, France

A detailed description of coupled heat and momentum transfer in a one-dimensional porous medium saturated by a supercritical fluid subject to a heat flux at one of its boundaries is reported in this study. The derivation is performed with an asymptotic analysis of the linearized macroscopic mass, momentum, and energy equations, assuming a van der Waals supercritical fluid and the mean-field theory, considering Darcy's law for momentum transfer. Three regimes of heat transfer separated by two crossovers are highlighted. The first regime, far enough from the critical point (CP), corresponds to the classical piston effect (PE), as in a plain fluid. While nearing the CP, a first crossover is found, giving rise to a second regime in which the PE in the bulk fluid is supplemented by a temperature gradient that results from a pressure gradient buildup. Below this crossover, the critical speeding up by thermocompression of the bulk stops and a *porous saturation* of the characteristic heat transfer timescale is reached. Closer to the CP, a second crossover is identified that corresponds to the presence of a viscous pressure drop in the whole domain. Below this second crossover, the PE is faded away and, in this third regime, heat transfer returns to a classical diffusive process. The two crossovers are characterized by a single parameter that is the ratio between the acoustic time (i.e., the sound wave travel time through a pore) and the pore-scale viscous diffusion time, namely, the acoustic pore Reynolds number.

DOI: [10.1103/PhysRevFluids.9.124402](https://doi.org/10.1103/PhysRevFluids.9.124402)

I. INTRODUCTION

The detailed understanding of relaxation rates of a disturbed supercritical fluid is very important for designing applications and/or analyzing natural phenomena where the temperature and pressure ranges can overlap the region of the gas-liquid critical point (CP). Far from the CP, it is classically assumed that a thermally disturbed fluid system will equilibrate with a diffusion relaxation time t'_D inversely proportional to the thermal diffusivity $D'_T = \Lambda' / (\rho' C'_p)$, where Λ' is the thermal conductivity and C'_p the specific heat at constant pressure. Introducing the correlation length ξ of the fluid density fluctuations near a liquid-gas CP [1], it is also well known that ξ exhibits a diverging power-law behavior such as $\xi \propto \tau^{-\nu}$ along the critical isochore. Here, ν is the universal critical exponent for the correlation length and $\tau = (T'_0 - T'_C) / T'_C$ is the dimensionless distance to

^{*}Contact author: didier.lasseux@cnrs.fr

the CP, T'_0 being the temperature of the fluid and T'_c its critical temperature. It should be recalled that $\nu = 0.63$ is the exact Ising value, while $\nu = 1/2$ is the corresponding mean-field value. Since C'_p and Λ' vary approximately as ξ^2 and ξ , respectively, it follows that $t'_D \propto D_T^{-1} \propto \xi$. This result implies that a diverging relaxation time $t'_D \propto \tau^{-\nu}$ will be observed for a fluid near its liquid-gas CP. This singular relaxation rate, known as the critical slowing down of the heat diffusion transport, was assumed to be correct for many ground-based experimental situations [2].

During the last two decades, more precise theoretical analyses [3–5] and experiments [6–9] performed near the CP of a constant-volume fluid cell have demonstrated that the faster relaxation rate of a disturbed pure fluid is due to the following adiabatic process. For a fixed volume sample, a rapid change in the boundary temperature leads to a thin boundary diffusion layer (called the thermal boundary layer (TBL) in the rest of this work) that acts like a piston to produce an adiabatic volume change within the sample core (the bulk fluid). This unusual adiabatic process came to be known as the piston effect (PE). After detailed pure thermodynamic analyses [6,7,10,11], direct simulation [8,12] and analytical one-dimensional (1D) solutions of the Navier-Stokes equations using the van der Waals equation of state [13–16], this new adiabatic relaxation behavior was definitively understood to become prominent. Indeed, it was recognized that near the CP, the divergence in the isothermal compressibility $\kappa'_T \propto C'_p \propto \tau^{-\nu}$, the isobaric thermal expansion $\alpha'_p \propto C'_p \propto \tau^{-\nu}$, and the specific heat ratio $C'_p/C'_v \propto \tau^{-\gamma-\alpha}$ near the gas-liquid CP lead to a critical speeding-up phenomenon. Here, γ and α are the universal critical exponents for the isothermal compressibility and the specific heat at constant volume, C'_v , respectively. As a matter of fact, with $C'_p \propto \xi^2$ and $\Lambda' \propto \xi$, approximately, and neglecting the small diverging behavior of C'_v , the relaxation rate t'_{PE} of the heat transport by PE tends to zero as $t'_{PE} \propto t'_D/(C'_p/C'_v)^2 \propto \xi^{-3} \propto \tau^{3\nu}$. The homogeneous pressure and temperature are typical features of the PE, except for temperature (and density) in the TBL. This last property motivated complementary theoretical approaches to describe the time evolution of temperature and density homogeneities in a microgravity and 1g environment [17,18]. Space experiments were performed confirming the fast temperature equilibration by the PE after a heating pulse [9] and the late-stage diffusive behavior of density changes during the final thermal equilibration of a closed fluid cell [19]. Recent experimental investigation of these phenomena has been reported in Ref. [20]. More details regarding the PE can be also found in Ref. [21].

The identification of the PE triggered a number of questions in the field of hydrodynamics of supercritical fluids which are Newtonian, viscous, and heat conducting fluids as dense as the corresponding liquid phase, as little viscous as the gas phase, and highly compressible [17]. Viscous effects are generally limited to thin boundary layers and do not affect much of the core flow. However, the assumption of a homogeneous pressure of the fluid sample in the early stages of the PE may fail close to the CP due to the divergence of the bulk viscosity which induces bulk spatial gradients [22,23]. Also, very close to the CP, the thermal equilibration time by PE can be shorter than the typical acoustic time [24]. Similarly, the boundary layer thickness can become less than the correlation length, a situation which has not been yet analyzed theoretically. Convection in closed cavities [12], hydrodynamic instabilities [25–29], and response to calibrated vibrations [30–33] have been addressed numerically or experimentally, under gravity and weightlessness conditions.

Whereas the specific properties of a near-critical fluid have motivated many developments in coupled heat and momentum transfer for a pure fluid [34,35], attention has barely been dedicated to the situation of a supercritical fluid saturated porous medium, although of fundamental importance. Applications in porous materials of major concern where the special characteristics of the supercritical fluid are exploited are numerous. This is the case for many processes in chemical engineering for which large mass diffusivity combined to a small viscosity is of particular interest. Applications, for example, are in chromatography, drying processes, fluid separation on porous columns, extraction or impregnation, crystallization, synthesis of ceramics, and particles of various materials ranging from nano- to macrodimensions [36–39]. For natural porous media, applications stem, for instance, from CO₂ storage in depleted hydrocarbon reservoirs or deep saline aquifers to petroleum recovery. The use of supercritical CO₂ in cooling devices like thermoacoustic systems

in which porous materials are involved has also been considered recently. In most existing reported work, the specific character of the supercritical fluid, particularly in near-critical conditions, and/or the coupling between hydrodynamics and heat transfer (namely, the work of pressure forces in the energy balance) is not taken into account [40–42]. A numerical investigation relying on a more thorough physical description was proposed in Ref. [43] where the coupled heat and mass transfer in a homogeneous porous medium saturated by a fluid close to its liquid-gas critical point was solved. More recently, a numerical approach was employed on a micromodel structure considered as an archetype of a model porous medium to analyze heat transfer during the transcritical path of CO₂ [44]. In this study, some results on the steady-state thermoconvective regime were shown in the presence of gravity in a two-dimensional porous layer. Some measurements carried out on a porous material saturated with a sub-, near-, and supercritical fluid were carried out, showing significant contrast in heat diffusivity [45]. In a weightlessness environment, heat transfer in a cavity filled with a near-critical fluid was found to be slower than the adiabatic transfer in a plain fluid in the same conditions. The slowing down was justified by the heat transfer from the fluid to the solid phase of the container.

Clearly, the specific hydrodynamics and associated coupled phenomena of a supercritical fluid together with the porous medium properties call upon a more detailed fundamental analysis for a better understanding and control of such a complex fluid-solid system. In particular our aim in the following work is to analyze whether the PE persists in porous media and, if this is the case, whether the associated scaling laws are modified by the presence of the porous matrix from which strong viscous effects might be expected due to shear within the pores. The analysis is carried out over a homogeneous 1D porous medium saturated by a van der Waals supercritical fluid while using a heuristic macroscopic model for the coupled heat and momentum transfer based on Darcy’s law, local thermal equilibrium, and mean-field theory. The problem is solved with the help of matched asymptotic expansions [46], the solution of which highlights a much richer phenomenology of heat transfer than in the case of a plain fluid. In fact, our analysis shows that, far enough from the CP, the piston effect exists as in the pure fluid. While nearing the CP, a first crossover is found below which pressure and temperature gradients appear in the bulk. Even closer to the CP, a second crossover is encountered characterized by pressure and temperature gradients in both the bulk and TBL. These overall results provide a frame to anticipate further fundamental developments on convection, stability in super- and subcritical conditions, as well on the design of innovative applications taking advantage of the specific features of the porous medium or near-critical fluid system.

With the aim of addressing the above questions, the paper is organized as follows. The physical model for the problem of coupled heat and momentum transfer in porous media along with the related assumptions are detailed in Sec. II. The solution to this problem is discussed in both the TBL (Sec. III) and the bulk (Sec. IV) before a closing description of the two crossovers given in Sec. V. The complete analysis shows three different regimes of heat transfer. An illustrative case example is developed in Sec. VI prior to concluding remarks reported in Sec. VII.

II. PHYSICAL MODEL

The configuration under study is that of a pair of parallel impermeable planes of infinite extensions and distant by L' , embedding a homogeneous nondeformable porous medium which pores are saturated by a near-(super)critical fluid. The system is supposed to be initially in thermodynamic equilibrium with the fluid at its critical density, ρ'_c , and a temperature $T'_0 > T'_c$ so that $\tau = (T'_0 - T')/T'_c \ll 1$. At $t' \geq 0$, the left boundary is heated with a flux $\phi'(t')$ yielding a coupled mechanism of heat and momentum transfer (see Fig. 1). In the rest of this paper, subscripts c and 0 are used to denote quantities in the fluid phase at the CP and at the initial conditions, respectively, whereas the prime variables are dimensional quantities. The analysis of the coupled heat, mass, and momentum transfer is carried out at the macroscopic scale, i.e., on the basis of an average description of the physical mechanism over a representative elementary volume of the saturated porous material. In the absence of a more detailed development of averaged equations, our analysis

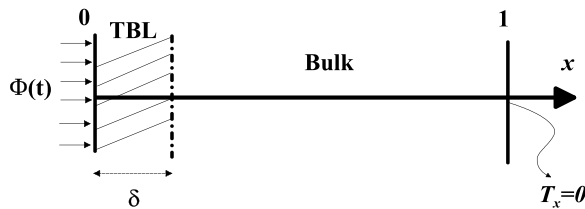


FIG. 1. The one-dimensional model with the TBL of thickness δ and the bulk. All quantities are indicated in their dimensionless form (see text for their definitions).

relies on the classical mass, momentum, and energy balance equations operating for classical fluids in porous media that are heuristically extended to the case involving a supercritical fluid. Under these circumstances, the macroscopic continuity equation for a compressible fluid is [47]

$$\rho' + (\rho' u')_{x'} = 0, \quad (1)$$

where ρ' is the local mean fluid density and u' is the interstitial velocity, both being mean values taken over the fluid volume in the porous medium (i.e., intrinsic phase averages). Subscripts t' and x' denote the partial derivatives with respect to time and space.

A complete form of the momentum balance equation derived in Ref. [48] may be considered, which is, however, rather complex for an analytical treatment. For tractability, a simplified version, corresponding to the unsteady form of Darcy's law that describes the creeping motion of a viscous fluid in a homogeneous porous medium at the macroscopic scale, is used [49]. This form assumes that the pressure gradient at the pore scale is small compared to that at the macroscopic scale and can be written as

$$\rho'[(u'_{t'} + f(u')u')] + P'_{x'} = -\frac{\mu'}{K'}\epsilon_p u', \quad (2)$$

where P' is the phase average fluid pressure, μ' is the shear viscosity, and ϵ_p the porosity, i.e., the ratio of the total accessible pore volume to the total volume of the sample. The term $\rho' f(u')u'$ in Eq. (2) is the Forchheimer correction to Darcy's law and represents the contribution of inertia to the macroscopic flow [50,51]. This term scales as u'^3 or u'^2 depending on the flow regime. The intrinsic permeability K' (m^2) is typically of the order of the square of the characteristic pore size and can typically vary from 10^{-19} m^2 for tight rocks to 10^{-9} m^2 for sintered materials for instance.

The choice for the equation of state results from a compromise between simplicity of the model and accuracy of the description. In the present case, the van der Waals equation of state is employed since its linearized form leads to relatively simple and phenomenologically sound scaling laws. For the thermophysical properties, real critical exponents could be used to give more accurate scaling laws (for comparison with experiments, for example), to the cost, however, of a much more cumbersome development. The van der Waals equation of state is expressed as

$$P' = \frac{\rho' r' T'}{1 - b' \rho'} - a' \rho'^2, \quad (3)$$

where T' is the intrinsic fluid phase average temperature. The two given constants a' and b' depend on the properties of the fluid under consideration (for CO_2 , $a' = 189 \text{ J m}^3 \text{ kg}^{-2}$ and $b' = 9.76 \times 10^{-4} \text{ m}^3 \text{ kg}^{-1}$, whereas $r' = 189 \text{ J kg}^{-1} \text{ K}^{-1}$).

For the energy balance, a one-temperature model including a term representing the work of pressure forces is used. By using such a model, local thermal equilibrium is assumed, which seems reasonable as justified in Ref. [43]. The model can be easily inferred from an analogous result previously derived for an incompressible fluid saturating a homogeneous porous medium under the local thermal equilibrium assumption [52]. In essence, the solid contribution to the energy balance only modifies the heat capacity and the thermal conductivity of the system. Using the

expression of the internal energy $E' = (C'_v)_{\text{eq}}T' - a'\rho'$ that follows from Eq. (3), the energy balance equation takes the form

$$(\rho'C'_v)_{\text{eq}}[T'_t + \epsilon_p u' T'_{x'}] = -\epsilon_p(P' + a'\rho'^2)u'_{x'} + (\Lambda'_{\text{eq}} T'_{x'})_{x'}, \quad (4)$$

where $(\rho'C'_v)_{\text{eq}} = \epsilon_p(\rho'C'_v)_{\text{fluid}} + (1 - \epsilon_p)\rho'_s C'_s$ denotes an equivalent specific heat for the fluid-saturated porous medium in which the subscript “s” stands for the solid phase. In addition, $\Lambda'_{\text{eq}} = \Lambda'_{\text{fluid}} \frac{2\epsilon_p}{(3-\epsilon_p)}$ is an effective heat conductivity for the fluid-saturated porous medium. This expression follows from Maxwell’s approximation [53]. In this expression, the contribution from the solid phase is omitted with the idea that it is negligible with respect to the diverging conductivity of the supercritical fluid [1]. The mean-field theory, which is the most consistent with the van der Waals equation of state, gives the heat conductivity for the supercritical fluid as $\Lambda'_{\text{fluid}} = \Lambda'_b + \Lambda_0^{\prime F} \tau^{-0.5} \cong \Lambda_0^{\prime F} \tau^{-0.5}$, where the background value Λ'_b can also be neglected compared to the diverging critical contribution $\Lambda_0^{\prime F} \tau^{-0.5}$.

The boundary and initial conditions reflect the above-mentioned 1D heat transport model and can be written as

$$u' = 0, \quad \text{at } x' = 0 \text{ and } x' = L', \quad (5a)$$

$$-\Lambda'_{\text{eq}} T'_{x'} = \Phi'(t'), \quad \text{at } x' = 0, \quad t' \geq 0, \quad (5b)$$

$$T'_{x'} = 0, \quad \text{at } x' = 1, \quad t' \geq 0, \quad (5c)$$

$$u'_0 = 0, \quad T'_0 = (1 + \tau)T'_c, \quad \rho'_0 = \rho'_c, \quad \text{at } t' < 0. \quad (5d)$$

Each dimensional quantity $\psi' = (T', \rho', P', u')$ is now rescaled under the form $\psi = \frac{(\psi' - \psi'_{\text{init}})}{\psi'_{\text{ref}}}$ where ψ'_{init} corresponds to the initial value and ψ'_{ref} is the reference value. The reference velocity, time, and pressure are taken as the values for the fluid in its ideal gas form. More precisely, u'_{ref} is the sound velocity, $u'_{\text{ref}} = c'_0 = \sqrt{\gamma_0 r' T'_{\text{ref}}}$, where $T'_{\text{ref}} = T'_c$ and γ_0 is the ratio of the specific heat coefficients for the fluid considered as an ideal gas. The reference time is the acoustic time $t'_a = L'/c'_0$ and the reference pressure is taken as $P'_{\text{ref}} = \rho'_{\text{ref}} r' T'_{\text{ref}}$. The reference density is $\rho'_{\text{ref}} = \rho'_c$. Length is made dimensionless by L' , i.e., $x = x'/L'$.

Replacing the different fluid properties and independent variables as functions of their respective nondimensional counterparts, the linearized dimensionless governing equations and associated boundary conditions can be written as follows:

$$\rho_t + u_x = 0, \quad (6a)$$

$$u_t + \gamma_0^{-1} P_x = -\frac{1}{\text{Re}_a \text{Da}} u, \quad (6b)$$

$$(\rho C_v)_{\text{eq}} T_t = -\frac{3}{2} u_x + \frac{\gamma_0}{\gamma_0 - 1} \frac{1}{\text{Pr}_0 \text{Re}_a} \tau^{-1/2} T_{xx}, \quad (6c)$$

$$P = \frac{3}{2} T + \frac{9}{4} \tau \rho. \quad (6d)$$

$$u(t, x) = 0, \quad \text{at } x = 0 \text{ and } x = 1, \quad (6e)$$

$$-\tau^{-1/2} T_x = \Phi(t), \quad \text{at } x = 0, \quad t \geq 0, \quad (6f)$$

$$T_x = 0, \quad \text{at } x = 1, \quad t \geq 0, \quad (6g)$$

$$\rho = u = T = P = 0, \quad \text{at } t < 0. \quad (6h)$$

In Eqs. (6b) and (6c), $\text{Re}_a = c'_0 L'/\nu'_0$ is the acoustic Reynolds number, with ν'_0 the kinematic viscosity of the fluid at the initial conditions. This dimensionless number represents the ratio of the characteristic viscous diffusion time to the acoustic propagation time in a fluid cavity of length

L' . For usual critical fluids $1/\text{Re}_a$ is a small parameter typically on the order of 10^{-8} ; larger values correspond to more viscous supercritical fluids. The Darcy number is defined as $\text{Da} = K'/(\epsilon_p L^2)$. The ratio $1/(\text{Re}_a \text{Da})$ can vary over several orders of magnitude (typically from 10^{-4} to 10^6 with $L' = 1$ cm) while $\frac{1}{(\text{Re}_a^2 \text{Da})}$ remains small compared to unity. In Eq. (6c), Pr_0 is an equivalent Prandtl number defined by $\text{Pr}_0 = \frac{v_0'}{D_{T_0}^{\text{eq}}}$, where $D_{T_0}^{\text{eq}}$ is an equivalent thermal diffusivity defined by $D_{T_0}^{\text{eq}} = \frac{2}{3-\epsilon_p} \Lambda_0^{\text{IF}} / (\rho_c' C_{p_0}')$, where $C_{p_0}' = \frac{\gamma_0}{\gamma_0-1} r'$ is the specific heat at constant pressure of the ideal gas. One should note that the mean-field theory yields a τ^{-1} divergence of the heat capacity at constant pressure [1] and thus a heat diffusivity which tends to zero as $\tau^{0.5}$. This implies that the sample heat diffusion characteristic time scales as $\sqrt{\tau}/\text{Re}_a$ with respect to the sample acoustic time. On the left-hand side of Eq. (6c), the term $(\rho C_v)_{\text{eq}}$ is the equivalent nondimensional product of the heat capacity at constant volume by the density of the fluid given by

$$(\rho C_v)_{\text{eq}} = \frac{(\rho' C_v')_{\text{eq}}}{\rho_c' r'} = \frac{1}{\gamma_0 - 1} + \frac{1 - \epsilon_p}{\epsilon_p} \rho_s C_s. \quad (7)$$

In this last relationship, $C_{v_0}' = C_{v_0}'/r' = 1/(\gamma_0 - 1)$ is the dimensionless heat capacity at constant volume of the near-critical fluid considered as a constant in the framework of the mean-field theory whereas $\rho_s C_s$ is the dimensionless product of the heat capacity by the density of the solid defined by $\rho_s C_s = \rho_s' C_s' / (\rho_c' r')$. In the boundary condition expressed in Eq. (6f) for the temperature, Φ is the dimensionless heat flux at $x = 0$, defined as $\Phi(t) = \Phi'(t) L' / (T_c' \Lambda_0^{\text{IF}})$.

At time $t = 0$, heat supply at $x = 0$ diffuses into the medium and the asymptotic analysis of the coupled equations on a given timescale ζ^{-1} (counted in sample acoustic time) is carried out. This timescale is that of the PE for the pure fluid that is much longer than the acoustic timescale and much shorter than the heat diffusion timescale [5], yielding the following hierarchy when Pr_0 is assumed of order 1:

$$\frac{\tau^{1/2}}{\text{Re}_a} \ll \zeta \ll 1. \quad (8)$$

This property defines a rescaled time variable $\theta = \zeta t$ which will be the basis of the development of the perturbed equations in the next section. Our goal is to analyze whether, like in plain supercritical fluids, a temperature equilibration timescale does exist which is much shorter than the sample heat diffusion time and how it is modified by the presence of the porous medium.

III. THERMAL BOUNDARY LAYER ANALYSIS

The domain is first divided into two subregions (see Fig. 1), namely, the thermal boundary layer (TBL) of dimensionless thickness δ and the bulk. Solution to the above set of balance equations is sought by carrying out matched asymptotic expansions in these two domains. The heat flux imposed at $x = 0$ and $t = 0$ induces perturbations on density, velocity, pressure, and temperature within the boundary layer. The respective first orders of magnitude of these perturbations are $\tilde{\eta}_\rho$, $\tilde{\eta}_u$, $\tilde{\eta}_P$, and $\tilde{\eta}_T$. The thickness of this TBL is of the order of magnitude of the heat penetration depth on the chosen timescale ζ^{-1} , and is thus much smaller than 1. Introducing the first-order expansions defined by $\rho = \tilde{\eta}_\rho \tilde{\rho}$, $u = \tilde{\eta}_u \tilde{u}$, $P = \tilde{\eta}_P \tilde{P}$, and $T = \tilde{\eta}_T \tilde{T}$ into the governing Eqs. (6) yields the first-order perturbation equations in the TBL that can be written as

$$\zeta \tilde{\eta}_\rho \tilde{\rho}_\theta + \delta^{-1} \tilde{\eta}_u \tilde{u}_z = 0, \quad (9a)$$

$$\zeta \tilde{\eta}_u \tilde{u}_\theta + \delta^{-1} \gamma_0^{-1} \tilde{\eta}_P \tilde{P}_z = -\frac{1}{\text{Re}_a \text{Da}} \tilde{\eta}_u \tilde{u}, \quad (9b)$$

$$(\rho C_v)_{\text{eq}} \zeta \tilde{\eta}_T \tilde{T}_\theta = -\frac{3}{2} \delta^{-1} \tilde{\eta}_u \tilde{u}_z + \frac{\gamma_0}{\gamma_0 - 1} \frac{1}{\text{Pr}_0 \text{Re}_a} \delta^{-2} \tilde{\eta}_T \tau^{-1/2} \tilde{T}_{zz}, \quad (9c)$$

$$\tilde{\eta}_p \tilde{P} = \frac{3}{2} \tilde{\eta}_T \tilde{T} + \frac{9}{4} \tau \tilde{\eta}_\rho \tilde{\rho}, \quad (9d)$$

$$-\delta^{-1} \tau^{-1/2} \tilde{\eta}_T \tilde{T}_z = \varphi W(\theta), \quad \text{at } z = 0, \theta \geq 0, \quad (9e)$$

$$\tilde{\rho} = \tilde{u} = \tilde{T} = \tilde{P} = 0, \quad \text{at } \theta < 0, \quad (9f)$$

$$\tilde{u}(z, \theta) = 0, \quad \text{at } z = 0, \quad (9g)$$

where $z = \delta^{-1}(x'/L') = \delta^{-1}x$ is the rescaled boundary layer space variable. The two terms on the right-hand side of the energy balance equation [Eq. (9c)] represent the perturbed form of the work of pressure forces $-(\frac{3}{2})\delta^{-1}\tilde{\eta}_u\tilde{u}_z$ and that of heat diffusion $\frac{\gamma_0}{\gamma_0-1} \frac{1}{\text{Pr}_0 \text{Re}_a} \delta^{-2} \tilde{\eta}_T \tau^{-1/2} \tilde{T}_{zz}$. In the boundary condition given by Eq. (9e), φ is the characteristic value of the boundary heat flux at the timescale θ and $0 \leq W(\theta) \leq 1$ is the time modulation.

A. Scaling analysis in the thermal boundary layer

The condition to keep the whole continuity equation of the compressible fluid is to match orders of magnitude of both terms in Eq. (9a), i.e.,

$$\zeta \tilde{\eta}_\rho = \delta^{-1} \tilde{\eta}_u, \quad (10)$$

so that the mass conservation equation can be rewritten as

$$\tilde{\rho}_\theta + \tilde{u}_z = 0. \quad (11)$$

The boundary condition given by Eq. (9e) for temperature readily gives the order of magnitude for the temperature in the TBL,

$$\tilde{\eta}_T = \delta \tau^{1/2} \varphi, \quad (12)$$

and Eq. (9e) can be also rewritten as

$$\tilde{T}_z = -W(\theta), \quad \text{at } z = 0, \theta \geq 0. \quad (13)$$

Coupling of the thermodynamic variables expressed in the equation of state (9d) gives the orders of magnitude for the pressure and density in the TBL according to

$$\tilde{\eta}_p = \tau \tilde{\eta}_\rho = \tilde{\eta}_T, \quad (14)$$

so that the equation of state becomes

$$\tilde{P} = \frac{3}{2} \tilde{T} + \frac{9}{4} \tilde{\rho}. \quad (15)$$

From Eqs. (10) and (14), it is clear that $\zeta \tilde{\eta}_T \ll \tilde{\eta}_u \delta^{-1}$ independently of the values of ζ and δ . When this is considered in the energy balance equation [Eq. (9c)], it follows that

$$\tilde{\eta}_u = \text{Re}_a^{-1} \delta^{-1} \tilde{\eta}_T \tau^{-1/2}, \quad (16)$$

so that the TBL energy balance equation can be written as

$$\frac{3}{2} \tilde{u}_z = \frac{\gamma_0}{\gamma_0 - 1} \frac{1}{\text{Pr}_0} \tilde{T}_{zz}. \quad (17)$$

Equations (10), (14), and (16) link space and timescales through the relation

$$\zeta \delta^2 = \text{Re}_a^{-1} \tau^{1/2}, \quad (18)$$

and provide the order of magnitude of the velocity in the TBL,

$$\tilde{\eta}_u = \text{Re}_a^{-1} \varphi. \quad (19)$$

B. A crossover to viscous effects in the boundary layer

Substituting the orders of magnitude for the pressure and velocity in the momentum balance equation [Eq. (9b)] leads to

$$\frac{\zeta}{\text{Re}_a} \tilde{u}_\theta + \gamma_0^{-1} \tau^{1/2} \tilde{P}_z = -\frac{1}{\text{Re}_a^2 \text{Da}} \tilde{u}. \quad (20)$$

In this equation, viscous effects are obviously negligible if

$$\tau^{1/2} \gg \frac{1}{\text{Re}_a^2 \text{Da}}. \quad (21)$$

Furthermore, if

$$\text{Da Re}_a \ll 1, \quad (22)$$

which will be assumed throughout this work, then the following relation holds,

$$\tau^{1/2} \gg \frac{1}{\text{Re}_a^2 \text{Da}} \gg \frac{1}{\text{Re}_a} \gg \frac{\zeta}{\text{Re}_a}, \quad (23)$$

and the unsteady term is always negligible in the momentum equation for the TBL.

It is thus clear that the condition expressed in Eq. (21) defines a crossover value, τ_{c2} , to viscous effects in the boundary layer on the τ scale. This crossover value is given by

$$\tau_{c2} = \left(\frac{1}{\text{Re}_a^2 \text{Da}} \right)^2. \quad (24)$$

At this point, it is important to note that

$$\text{Re}_a^2 \text{Da} = \left(\frac{c'_0 \sqrt{\frac{K'}{\epsilon_p}}}{v'_0} \right)^2 = \text{Re}_p^2, \quad (25)$$

which defines the acoustic pore Reynolds number, Re_p , with $\sqrt{\frac{K'}{\epsilon_p}}$ the characteristic length at the pore scale (i.e., the pore diameter). This dimensionless number is nothing else than the ratio between the viscous diffusion time and acoustic time at the pore scale and simply leads to $\tau_{c2} = 1/\text{Re}_p^4$. This indicates that τ_{c2} increases with increasing viscosity and decreasing pore size. However, unless the porous material is very weakly permeable, this value can be very close to the CP for some supercritical fluids so that the description of the fluid motion by the Navier-Stokes equations at the microscale can be questionable. For instance, for CO₂ ($T'_c = 304.13$ K, $\mu'_0 = 1.37 \times 10^{-5}$ kg m⁻¹ s⁻¹, $\rho'_c = 467.8$ kg m⁻³, $c'_0 \approx 265$ m s⁻²) saturating a porous material having the characteristics $\epsilon_p = 0.2$, $K' = 3 \times 10^{-18}$ m², this crossover is at about 2×10^{-4} K from the critical temperature. It should be noted, however, that this crossover value depends on the fourth power of the viscosity and may thus be farther from the CP for much viscous fluids.

If condition (21) is fulfilled, the momentum balance equation reduces to

$$\tilde{P}_z = 0. \quad (26)$$

As a consequence, when $\tau \gg \tau_{c2}$, the governing equations in the boundary layer [Eqs. (11), (15), (17), and (26)] are the same as for plain critical fluids [15]. The solution of this set of equations with the boundary condition given in Eq. (13) is recalled in Appendix A. Heat deposited at the boundary of the medium diffuses within the TBL, which expands due to the strong compressibility of the fluid, inducing a large compression of the fluid in the bulk region which is analyzed in the next section.

IV. THE BULK ANALYSIS

The nonvanishing fluid velocity at the edge of the TBL generates density, velocity, pressure, and temperature perturbations in the bulk of respective first orders of magnitude $\bar{\eta}_\rho$, $\bar{\eta}_u$, $\bar{\eta}_P$, and $\bar{\eta}_T$. Introducing the first-order expansions $\rho = \bar{\eta}_\rho \bar{\rho}$, $u = \bar{\eta}_u \bar{u}$, $P = \bar{\eta}_P \bar{P}$, and $T = \bar{\eta}_T \bar{T}$ into the governing Eqs. (6) leads to the first-order perturbation equations in the bulk that can be written as follows:

$$\zeta \bar{\eta}_\rho \bar{\rho}_\theta + \bar{\eta}_u \bar{u}_x = 0, \quad (27a)$$

$$\zeta \bar{\eta}_u \bar{u}_\theta + \gamma_0^{-1} \bar{\eta}_P \bar{P}_x = -\frac{1}{\text{Re}_a \text{Da}} \bar{\eta}_u \bar{u}, \quad (27b)$$

$$(\rho C_v)_{\text{eq}} \zeta \bar{\eta}_T \bar{T}_\theta = -\frac{3}{2} \bar{\eta}_u \bar{u}_x + \frac{\gamma_0}{\gamma_0 - 1} \frac{1}{\text{Pr}_0 \text{Re}_a} \bar{\eta}_T \tau^{-1/2} \bar{T}_{xx}, \quad (27c)$$

$$\bar{\eta}_P \bar{P} = \frac{3}{2} \bar{\eta}_T \bar{T} + \frac{9}{4} \tau \bar{\eta}_\rho \bar{\rho}, \quad (27d)$$

$$\bar{\rho} = \bar{u} = \bar{T} = \bar{P} = 0, \quad \text{at } \theta < 0, \quad (27e)$$

$$\bar{u}(x, \theta) = 0, \quad \text{at } x = 1, \quad (27f)$$

$$\bar{T}_x(x, \theta) = 0, \quad \text{at } x = 1. \quad (27g)$$

Boundary conditions at $x = 0$ are replaced by the matching conditions with the boundary layer which, at the first order, are simply given by $\lim_{z \rightarrow \infty} \tilde{\eta}_\psi \tilde{\psi}(z, \theta) = \bar{\eta}_\psi \bar{\psi}(x = 0, \theta)$ ($\psi = (T, \rho, P, u)$).

A. Scaling analysis in the bulk

From Eqs. (A4)–(A8), $\tilde{P}(z, \theta)$, $\tilde{T}(z, \theta)$, and $\tilde{u}(z, \theta)$ tend to a finite value at the edge of the boundary layer, whereas $\tilde{\rho}(z, \theta)$ tends to zero, from which it can be deduced that

$$\bar{\eta}_T = \tilde{\eta}_T, \quad \bar{\eta}_P = \tilde{\eta}_P, \quad \bar{\eta}_u = \tilde{\eta}_u, \quad \bar{\eta}_\rho \ll \tilde{\eta}_\rho. \quad (28)$$

Balancing both terms in the mass conservation equation [Eq. (27a)] in the bulk implies

$$\zeta \bar{\eta}_\rho = \bar{\eta}_u, \quad (29)$$

and hence the mass conservation in the bulk is

$$\bar{\rho}_\theta + \bar{u}_x = 0. \quad (30)$$

Matching the transient term with the largest term that expresses the work of pressure forces in the energy balance equation [Eq. (27c)] in the bulk yields

$$\zeta \bar{\eta}_T = \bar{\eta}_u, \quad (31)$$

and consequently the energy balance in the bulk is given by

$$(\rho C_v)_{\text{eq}} \bar{T}_\theta = -\frac{3}{2} \bar{u}_x. \quad (32)$$

The coupling between temperature and pressure in the equation of state implies

$$\bar{\eta}_P = \bar{\eta}_T, \quad (33)$$

and taking into account the relation in Eq. (28) for $\bar{\eta}_\rho$ gives the approximate equation of state in the bulk,

$$\bar{P} = \frac{3}{2} \bar{T}. \quad (34)$$

The relationship given by Eq. (31), together with those reported in Eqs. (28), (12), and (19), gives

$$\zeta \delta = \frac{\tau^{-1/2}}{\text{Re}_a}. \quad (35)$$

Taking into account the expression provided by Eq. (18) yields

$$\delta = \tau, \quad (36)$$

which, once inserted back into Eq. (35), provides the timescale for the PE,

$$\zeta = \frac{\tau^{-3/2}}{\text{Re}_a}. \quad (37)$$

The various orders of magnitude are

$$\bar{\eta}_T = \bar{\eta}_P = \tilde{\eta}_T = \tilde{\eta}_P = \tau^{3/2} \varphi, \quad \tilde{\eta}_\rho = \tau^{1/2} \varphi, \quad \bar{\eta}_\rho = \tau^{3/2} \varphi. \quad (38)$$

It should be noted here that the relationship given in Eq. (37), and the definition of the rescaled time variable $\theta = \zeta t$, indicate that, as far as $\tau \gg \frac{1}{\text{Re}_a^{2/3}}$, a constraint that is assumed to be satisfied in the sequel of this paper, the following hierarchy holds:

$$\frac{\tau^{1/2}}{\text{Re}_a} \ll \frac{1}{\text{Re}_a} \ll \zeta = \frac{\tau^{-3/2}}{\text{Re}_a} \ll 1. \quad (39)$$

This means that the heat equilibration timescale is shorter than the heat diffusion timescale in the ideal gas but longer than the acoustic characteristic time of the plain fluid cavity.

B. A crossover to viscous effects in the bulk

Substituting expressions given in Eqs. (36)–(38) into the momentum balance equation [Eq. (27b)] gives

$$\frac{1}{\text{Re}_a^2 \tau^{3/2}} \bar{u}_\theta + \tau^{3/2} \frac{\bar{P}_x}{\gamma_0} = -\frac{1}{\text{Re}_a^2 \text{Da}} \bar{u} = -\frac{1}{\text{Re}_p^2} \bar{u}. \quad (40)$$

Evidently, if $\tau \gg \left(\frac{1}{\text{Re}_a^2 \text{Da}}\right)^{2/3} = \frac{1}{\text{Re}_p^4}$, keeping in mind the conditions $\text{Da} \text{Re}_a \ll 1$ and $\tau \gg \frac{1}{\text{Re}_a^{2/3}}$, the following hierarchy holds,

$$\frac{1}{\text{Re}_a \tau^{3/2}} \ll \text{Re}_a \text{Da} \ll \frac{1}{\text{Re}_a \text{Da}} \ll \text{Re}_a \tau^{3/2}, \quad (41)$$

and Darcy's equation in the bulk also reduces to

$$\bar{P}_x = 0. \quad (42)$$

This obviously defines another crossover τ_{c1} on τ given by

$$\tau_{c1} = \left(\frac{1}{\text{Re}_a^2 \text{Da}}\right)^{2/3} = \frac{1}{\text{Re}_p^4}, \quad (43)$$

below which viscous effects become significant in the bulk.

As a consequence, when $\tau \gg \tau_{c1}$, the governing equations are exactly the same as those for the plain supercritical fluid [5,15] and the solution in the bulk displays homogeneous temperature, pressure, and density which are reported in Appendix A. It should be noted here that the system of Eqs. (30), (32), and (34) yields a first-order equation in space for the energy equation in the above first-order expansion analysis. This implies that the thermal boundary condition at $x = 1$ in Eq. (27g) is not necessary because mechanisms occurring at the acoustic timescale have been filtered out by using the PE timescale. This timescale, ζ , on which temperature in the sample is

homogenized by thermocompressive heating, decreases to zero as $\tau^{3/2}$. Thus, it is much smaller than the heat diffusion time, which increases to infinity as $\tau^{-1/2}$ [5]. This critical speeding up of the heat transfer contrasts with the critical heat diffusion slowing down. In other words, as far as the condition $\tau \gg 1/\text{Re}_p^{4/3}$ is fulfilled, the PE is not affected by the porous matrix. In this case, the solution that is uniformly valid in both the TBL and bulk is provided in Appendix A [see Eqs. (A13)–(A16)].

When nearing the CP so that τ becomes close to $\tau_{c1} = 1/\text{Re}_p^{4/3}$, a pressure gradient, compensated by viscous shear, builds up in the bulk. As for τ_{c2} , this value depends only on the pore-scale characteristic length $\sqrt{\frac{K'}{\epsilon_p}}$ for a given fluid. For carbon dioxide and the same characteristic values of the porous material as those considered for τ_{c2} , this crossover value to the viscous effect of the porous material on the PE is at about 2.5 K above the critical temperature.

As a summary, it must be emphasized that both crossovers τ_{c1} and τ_{c2} are only functions of the ratio between the pore-scale acoustic wave travel time, $\frac{\sqrt{K'}}{c_0}$, and the pore-scale viscous diffusion time, $(\frac{K'}{\epsilon_p})/v'_0$, that is, the inverse of the acoustic pore Reynolds number, Re_p [see Eq. (25)]. More specifically, τ_{c1} varies as $1/\text{Re}_p^{4/3}$, whereas τ_{c2} depends on $1/\text{Re}_p^4$. For a fixed fluid, the crossovers are therefore solely dependent upon the characteristic pore size $\sqrt{K'/\epsilon_p}$ and they decrease when the pore size increases. The physical significance of this behavior lies in the fact that when the contrast between the acoustic wave travel time and viscous diffusion time increases (this is favored by large pores), viscous effects relax at a characteristic time that is much larger than the time of travel of the thermocompressive wave. Consequently, viscous dissipation and thermoacoustic heat transfer do not overlap. However, if τ is sufficiently decreased (down to values smaller than τ_{c1}), viscous effects become important enough to counteract the fluid expansion.

V. ANALYSIS OF THE CROSSOVERS

As shown in the previous sections, when the distance to the CP, τ , approaches τ_{c1} (or even closer to the CP, when $\tau \sim \tau_{c2}$), the pressure gradient and the viscous shear in Darcy's law become of the same order of magnitude (in the bulk for τ_{c1} as well as in the TBL for τ_{c2}). The pressure gradient becomes of first order in the pressure asymptotic expansion which is thus no longer well ordered. Accordingly, the asymptotic expansions, as performed in the previous section, are singular for the values τ_{c1} and τ_{c2} of the small parameter τ . As a consequence, they no longer correctly approximate the solutions of the governing equations, and crossover-type solutions, sometimes also named inner descriptions [15], are needed. These crossover-type expansions are obtained for $\tau \rightarrow 0$ with a fixed value of the crossover parameter $\tilde{\tau}_i$ defined by the ratio $\tilde{\tau}_i = \tau/\tau_{ci}$ (index $i = 1, 2$ corresponds to one of the crossover values). The crossover solutions presented below are obtained following the same procedure as the one detailed in the previous section.

A. First crossover

In this section, the solution when τ is close to τ_{c1} is reinspected. An inner description is necessary where $\tilde{\tau}_1 = \tau/\tau_{c1}$ is kept of order 1 while $\tau \rightarrow 0$. In this limit of τ , i.e., $1/\text{Re}_p^2 \ll 1$ (which further means that, due to the condition given by Eq. (22), $\frac{1}{\text{Re}_a} \ll \text{Re}_a \text{Da} \ll 1$), and because the solution presented above is singular when $1/\text{Re}_p^2$ is zero, the development must be carried out again. This can be performed in a similar way as the one detailed in the previous sections, except τ_{c1} is now kept in the orders of magnitude equations while $\tilde{\tau}_1$ remains in the balance equations. When this is done, the following orders of magnitude are obtained:

$$\tilde{\eta}_T = \tilde{\eta}_p = \bar{\eta}_T = \bar{\eta}_p = \bar{\eta}_\rho = \tau_{c1}^{3/2} \varphi, \quad \tilde{\eta}_\rho = \tau_{c1}^{1/2} \varphi, \quad \tilde{\eta}_u = \bar{\eta}_u = \varphi/\text{Re}_a. \quad (44)$$

Moreover, the TBL thickness is obtained as $\delta = \tau_{c1}$, and the timescale parameter is $\zeta = \text{Re}_a \text{Da}$. The condition given by Eq. (22) thus becomes a necessary condition for the equilibration time to be longer than the acoustic time. Here, it must be noticed that the PE characteristic time is no longer decreasing with τ . It keeps a constant value independent of the distance, τ , to the CP. This is in contrast with the pure PE above the crossover to viscous effects in the bulk [cf. Eq. (37)]. This phenomenon will be referred to as the *porous saturation* of the PE. Indeed, above the first crossover, i.e., for $\tau^{3/2} > \frac{1}{\text{Re}_p^2}$, the PE timescale is $\theta_{PE} = \frac{1}{\text{Re}_a} t / \tau^{3/2}$ while, at the first crossover, $\theta = \frac{1}{\text{Re}_a} t / \frac{1}{\text{Re}_p^2}$. This shows that the porous saturation timescale θ of the PE is a longer timescale than the pure piston effect timescale θ_{PE} . At the crossover, the PE, which is, however, slowed down by the effect of the porous matrix, still speeds up heat transfer compared to diffusion.

As far as the condition expressed in Eq. (21) is fulfilled, pressure remains homogeneous in the TBL, the expansion of which is not affected by the porous medium, whereas a pressure gradient becomes significant in the bulk. The overall set of balance equations in both the TBL and the bulk as well as the uniformly valid solutions for density, temperature, velocity, and pressure are reported in Appendix B. It can be easily verified that these solutions exactly match those corresponding to the PE reported above in the limit $\tilde{\tau}_1 \rightarrow \infty$.

As expected, the TBL remains purely diffusive while a temperature (and pressure) gradient takes place in the bulk which physical origin lies in the viscous dissipation due to the porous matrix. The dissipation itself originates from significant viscous shear within the pores when τ is close to τ_{c1} , yielding a macroscopic pressure gradient as described by Darcy's law during partial reflections of acoustic waves emitted by the expanding fluid contained in the TBL. This last feature has to be checked by direct numerical solutions of the equations at the acoustic timescale as was done for the PE in a plain supercritical fluid [12]. Interestingly, it should be noted that only the boundary layer part of the solution explicitly depends on the crossover parameter $\tilde{\tau}_1$; the bulk part, at the timescale θ , is written only in terms of the two kernels $K_T(x, v)$ and $K_u(x, v)$ [Eqs. (B17) and (B21)], which do not involve $\tilde{\tau}_1$. This result comes from the fact that conservation equations in the bulk are independent of $\tilde{\tau}_1$ and that the velocity at the outer edge of the TBL is constant and equal to $\frac{2}{3}AW(\theta)$. In comparison to the PE previously investigated, the first crossover leads to a time rescaling and the superposition of the bulk pressure and temperature gradients which are independent of the distance to the CP near τ_{c1} .

In the present inner description, the viscous pressure drop was neglected in the TBL since this term is τ_{c1} smaller than \tilde{p}_z . If this term were, however, kept in the description, the diffusion coefficient for \tilde{p} (and \tilde{T}) would be given by $A\tilde{\tau}_1 / (1 + \frac{4}{9}A\gamma_0\tau_{c1}\tilde{\tau}_1^{-1/2})$. Approximating this coefficient by $A\tilde{\tau}_1$, as was done in the present crossover analysis, remains valid when $\tilde{\tau}_1$ is decreased until it reaches a value such that $\tau_{c1}\tilde{\tau}_1^{-1/2} \sim 1$, i.e., when $\tilde{\tau} = \tau/\tau_{c1} \sim \tau_{c1}^2$, which means $\tau \sim \tau_{c1}^3 = \tau_{c2}$. As expected, the inner description detailed above must hence be revisited while nearing the CP with τ close to τ_{c2} , in which circumstances a second crossover analysis must be performed. This is the purpose of the following section.

B. Second crossover

When nearing the CP much closer than τ_{c1} , the already-mentioned value $\tau \sim \tau_{c2} = 1/\text{Re}_p^4$ may be reached for which the pressure gradient reaches the TBL and this requires the inner description to be reconsidered with $\tilde{\tau}_2 = \tau/\tau_{c2}$. At this crossover, fluid expansion in the TBL will be weakened due to viscous effects, suggesting that the PE will be strongly affected. The procedure to obtain this second crossover solution is similar to that already used for the first one and it is sufficient to only report the main results. The orders of magnitude are given by

$$\tilde{\eta}_T = \tilde{\eta}_p = \tau_{c2}\varphi, \quad \tilde{\eta}_\rho = \varphi, \quad \tilde{\eta}_u = \bar{\eta}_u = \frac{\varphi}{\text{Re}_a}, \quad \bar{\eta}_T = \bar{\eta}_p = \bar{\eta}_\rho = \tau_{c2}^{1/2}\varphi. \quad (45)$$

The TBL thickness is now $\delta = \tau_{c2}^{1/2} = 1/\text{Re}_p^2$ while the timescale is unchanged with respect to the first crossover, i.e., $\zeta = \text{Re}_a \text{Da}$. Conservation equations and uniformly valid solutions are reported

TABLE I. Thermophysical parameters of the supercritical fluid (CO₂) and properties of the porous medium (whose solid skeleton is made of aluminum oxide) used for the case example.

Fluid (CO ₂)		Porous medium (aluminum oxide)	
T'_c (K)	304.14	ρ'_s (kg m ⁻³)	3390
ρ'_c (kg m ⁻³)	467.8	K' (m ²)	3×10^{-18}
P'_c (MPa)	7.37	ϵ_p (-)	0.2
r' (J kg ⁻¹ K ⁻¹)	189	C'_s (J kg ⁻¹ K ⁻¹)	850
C'_{p0} (J kg ⁻¹ K ⁻¹)	819		
$\gamma_0 = C'_{p0}/C'_{v0}$ (-)	1.3		
ν'_0 (m ² s ⁻¹)	2.93×10^{-8}		
Λ_0^{rF} (W m ⁻¹ K ⁻¹)	3.38×10^{-3}		

in Appendix C. In the limit $\tilde{\tau}_2 \rightarrow \infty$ for which $A_2(\tilde{\tau}_2) \sim A\tilde{\tau}_2^{1/2} = A_1(\tilde{\tau}_2)$ [see Eq. (C16) for the definition of $A_2(\tilde{\tau}_2)$], it can be easily verified that these solutions are identical to those at the first crossover.

The solution $T(x, t)$ [see Eq. (C18)] clearly indicates that the PE is strongly weakened. The physical mechanisms of the fading away of the PE can be explained by the solution $\tilde{u}(z, \theta)$ for the velocity in the TBL that is given by

$$\tilde{u}(z, \theta) = \frac{2}{3}A_2(\tilde{\tau}_2)\tilde{\tau}_2^{-1/2} \left(W(\theta) - \int_0^\theta \frac{z}{2\sqrt{\pi A_2(\tilde{\tau}_2)v^3}} \exp\left(-\frac{z^2}{4A_2(\tilde{\tau}_2)v}\right) W(\theta - v) dv \right). \quad (46)$$

The fluid expanding velocity at the outer edge of the TBL is such that $\tilde{u}_\infty(\theta) = \lim_{z \rightarrow \infty} \tilde{u}(z, \theta) = \frac{2}{3}A_2(\tilde{\tau}_2)\tilde{\tau}_2^{-1/2}W(\theta)$ which is obviously decreasing to zero as $\tilde{\tau}_2^{1/2}$. This clearly demonstrates that the PE is faded away by viscous shear in the TBL that thwarts fluid expansion and yields a progressive return to heat transfer by diffusion. The strong dependence of $\tilde{u}_\infty(\theta)$ on $\tilde{\tau}_2$ generates gradients in the bulk part of the solution. These gradients are strongly dependent on the distance to the CP near τ_{c2} , a feature that contrasts with the behavior near τ_{c1} .

VI. CASE EXAMPLE

This section is dedicated to an illustration of the above predictions of the three different regimes of heat transfer. This is carried out in a one-dimensional porous domain saturated by a near-critical fluid. The porous matrix and fluid properties are reported in Table I.

The three regimes with the two crossovers which have been theoretically characterized in the previous sections are the following (see Fig. 2):

Regime (I): When $\tau \gg \tau_{c1} = 1/\text{Re}_p^{4/3}$, the PE dominates and heat propagates like in a pure supercritical fluid, regardless the presence of the porous matrix. This regime can be called *pure PE*.

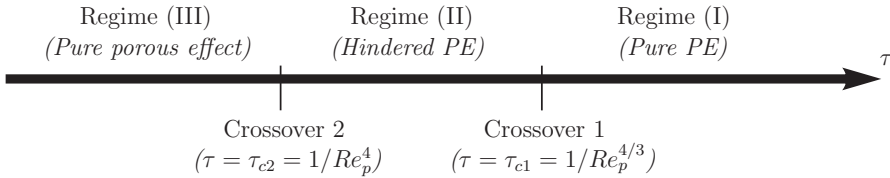


FIG. 2. Heat transfer regimes depending on the distance, τ , to the critical point. The three regimes are separated by two crossovers, $\tau_{c1} = 1/\text{Re}_p^{4/3}$ and $\tau_{c2} = 1/\text{Re}_p^4$. Regime (I) ($\tau \gg \tau_{c1}$) corresponds to the *pure PE*. Regime (II) ($\tau_{c2} < \tau < \tau_{c1}$) is where viscous effects counteract the thermoacoustic heat transfer in a so-called *hindered PE*. Regime (III) corresponds to heat transfer by diffusion (*pure porous effect*).

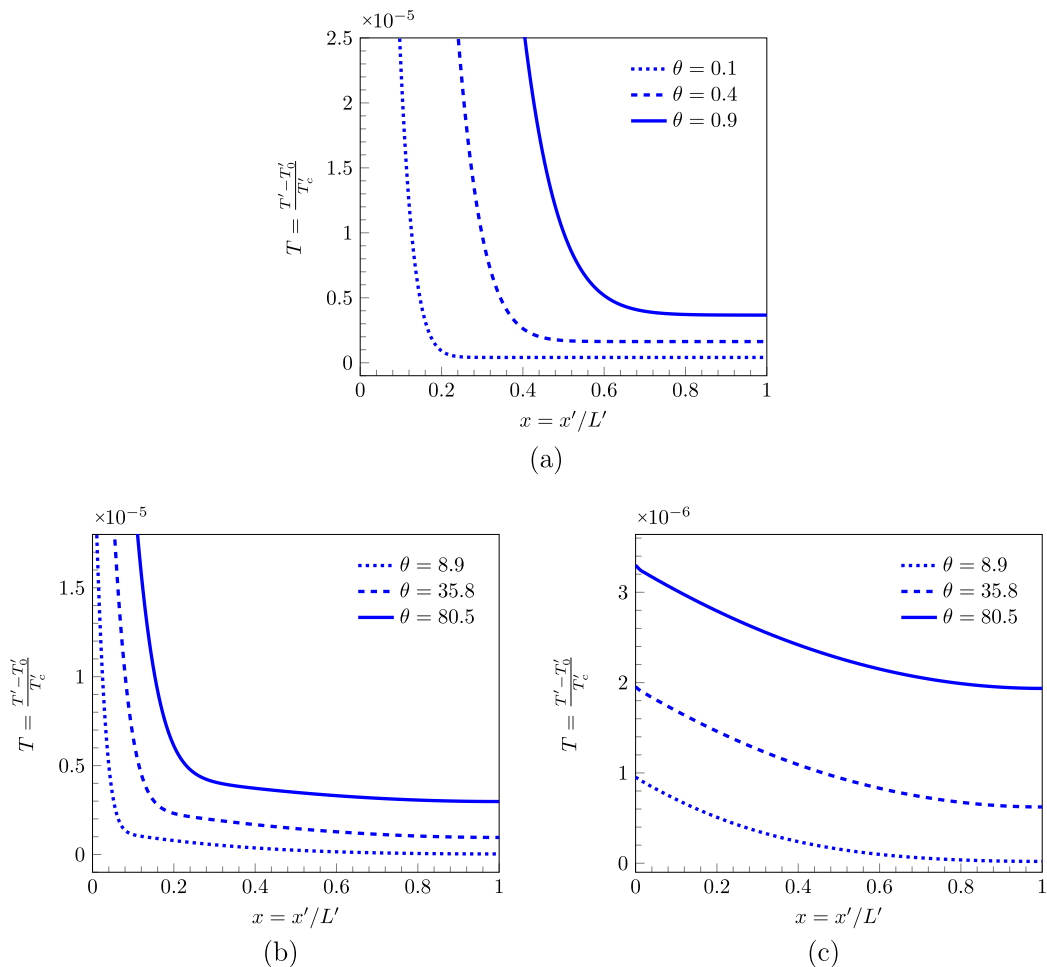


FIG. 3. Dimensionless temperature perturbation profiles as a function of x for three different dimensionless times, θ , corresponding to the same values of t : $t = 0.1\text{Re}_a\tau^{3/2}$, $t = 0.4\text{Re}_a\tau^{3/2}$, and $t = 0.9\text{Re}_a\tau^{3/2}$ in which τ is the one used in (a), i.e., $\tau = 20\tau_{c1}$: (a) regime (I), pure PE [solution from Eq. (A14)], $\tau = 20\tau_{c1}$; (b) regime (II), hindered PE at $\tau = \tau_{c1}$ [solution from Eq. (B19)]; and (c) regime (III), pure porous effect at $\tau = \tau_{c2}$ [solution from Eq. (C18)]. Physical parameters are recalled in Table I.

PE. When τ becomes of the order of τ_{c1} , a temperature (and pressure) gradient appears in the bulk, the features of the TBL being unmodified.

Regime (II): This regime between the two crossovers is characterized by the presence of pressure and temperature gradients in the bulk superimposed to the PE. This regime can be referred to as *hindered PE*. While decreasing τ close enough to $\tau_{c2} = 1/\text{Re}_a^4$, the viscous pressure gradient reaches the TBL and thermal diffusion effects become important in the overall medium.

Regime (III): When τ is decreased below τ_{c2} , the PE fades away progressively and heat transfer is completely governed by diffusion. This regime can be called *pure porous effect*.

The porous medium has a length $L' = 1$ mm leading to $\text{Re}_a \approx 9.3 \times 10^6$, $\text{Da} = 1.5 \times 10^{-11}$, and $\text{Re}_p = 36$ while the two crossover values are $\tau_{c1} \approx 8.37 \times 10^{-3}$ and $\tau_{c2} \approx 5.87 \times 10^{-7}$. A heat flux $\Phi'(t') = 10 \text{ W m}^{-2}$ (yielding $\varphi = 0.01$ and $W(\theta) = 1$) is applied at $x = 0$. The resulting dimensionless temperature perturbations along the porous domain ($0 \leq x \leq 1$) are reported in Fig. 3, for three different dimensionless times and for three values of τ corresponding to each of

the three regimes: (I) Fig. 3(a), (II) Fig. 3(b), and (III) Fig. 3(c). The three dimensionless times are identical and correspond to $t = 0.1\text{Re}_d\tau^{3/2}$, $t = 0.4\text{Re}_d\tau^{3/2}$, and $t = 0.9\text{Re}_d\tau^{3/2}$ in which τ is the one used in Fig. 3(a), i.e., $\tau = 20\tau_{c1}$. Solutions in Figs. 3(b) and 3(c) are obtained with $\tilde{\tau}_1 = 1$ and $\tilde{\tau}_2 = 1$, respectively.

In Fig. 3(a), results correspond to the pure PE, in accordance with previous studies in a plain fluid cavity [5,15] and for which the two distinct zones are clearly apparent: (i) a boundary layer, which grows with time, where diffusion effects are dominant, and (ii) a homogeneous bulk temperature resulting from the PE which increases with time. In contrast, the temperature perturbation profiles in Fig. 3(b) do not correspond to the pure PE regime, exhibiting two main features: (i) a thin and time growing TBL remains at $x = 0$; (ii) a temperature gradient, which originates from the pressure gradient in the bulk region, settles down, starting from the outer edge of the TBL. This gradient progressively develops and spreads over the whole region of the bulk. Finally, the temperature perturbation fields for $\tau = \tau_{c2}$ represented in Fig. 3(c) show no PE as they rather correspond to diffusive profiles. The pressure gradient that reaches the TBL contributes to fade away the PE thus preventing heat propagation at constant temperature by thermoacoustic effects.

VII. CONCLUSION

A complete one-dimensional asymptotic analysis has been performed within the framework of the mean-field theory and the classical Darcy model in order to analyze the coupled heat and momentum transfer in a one-dimensional homogeneous porous medium saturated by a supercritical fluid and subjected to a heat flux at one edge. This analysis shows that heat transfer is characterized by three distinct regimes, separated by two crossovers, τ_{c1} and τ_{c2} . These crossovers only depend on

the acoustic pore Reynolds number defined as $\text{Re}_p = \frac{c'_0\sqrt{K'}}{v'_0}$ and τ_{c1} and τ_{c2} vary with this parameter according to a $-4/3$ and -4 power law, respectively. When the temperature of the fluid is such that τ is significantly larger than τ_{c1} , heat transfer occurs as in a plain supercritical fluid by PE: a TBL develops at the heated edge of the medium, the expansion of which leads to a thermocompressive heating of the bulk featuring a constant pressure and temperature ahead of the boundary layer. When τ is of the same order or smaller than τ_{c1} , viscous stress within the bulk becomes significant enough to oppose the fluid expansion: pressure and temperature gradients resulting from viscous dissipation build up in the bulk where heat diffusion and the piston effect are superimposed. This first crossover also corresponds to a critical speeding up standstill of the PE. Indeed, the characteristic PE timescale becomes constant, a phenomenon that can be referred to as a porous saturation of the PE. While further decreasing τ to or below τ_{c2} , the viscous shear stress becomes also significant in the boundary layer and the piston effect is faded away.

This analysis clarifies some of the fundamental aspects of coupled heat and momentum transfer in a near-(super)critical fluid-saturated porous medium and should serve as the basis of further investigations including the validation of the proposed theory by the development of numerical solutions at the pore scale that is out of the scope of the present work. It also opens the way for many other physical implications, including instabilities, the role of a body force (gravity), and, in two-phase flow, the coupling with capillary effects.

ACKNOWLEDGMENTS

This project has received financial support from the Centre National de la Recherche Scientifique (CNRS) through the MITI interdisciplinary programs and its exploratory research project TSCOOP. The RRI BEST-Usine du futur (factory of the future) of the University of Bordeaux as well as the French ‘‘Centre National d’Etudes Spatiales’’ (CNES) and CNRS through the research group ‘‘Micropesanteur Fondamentale et Appliquée’’ are also gratefully acknowledged.

APPENDIX A: SOLUTIONS IN THE PURE PE REGIME

This appendix reports on the solutions for $\tilde{\rho}$, \tilde{T} , \tilde{u} , and \tilde{p} in the TBL when $\tau \gg \tau_{c2}$ and for $\bar{\rho}$, \bar{T} , \bar{u} , and \bar{p} in the bulk when $\tau \gg \tau_{c1}$, corresponding to the classical PE.

1. TBL

The procedure starts with the solution of the diffusion equation on $\tilde{\rho}$ which is obtained by combining Eqs. (11), (15), (17), and (26), yielding

$$\tilde{\rho}_\theta = A\tilde{\rho}_{zz}, \quad (\text{A1})$$

where

$$A = \frac{\gamma_0}{\gamma_0 - 1} \text{Pr}_0^{-1}. \quad (\text{A2})$$

The associated boundary condition follows from Eqs. (13), (15), and (26) and is given by

$$\tilde{\rho}_z(z = 0, \theta) = -\frac{2}{3}\tilde{T}_z(z = 0, \theta) = \frac{2}{3}W(\theta), \quad (\text{A3})$$

while the initial condition is given by Eq. (9f). Using the fact that $\tilde{\rho}$ is bounded for $z \in [0, 1]$, the solution is

$$\tilde{\rho}(z, \theta) = -\frac{2}{3}A \int_0^\theta K_\rho(z, v)W(\theta - v)dv, \quad (\text{A4})$$

which involves the normalized diffusion kernel for density, $K_\rho(z, v)$:

$$K_\rho(z, v) = \frac{1}{\sqrt{\pi Av}} \exp\left(-\frac{z^2}{4Av}\right). \quad (\text{A5})$$

Taking now into account the equation of state (15) and the homogeneous character of the pressure in the boundary layer [Eq. (26)], Eq. (A4) gives the temperature field,

$$\tilde{T}(z, \theta) = A \int_0^\theta K_\rho(z, v)W(\theta - v)dv + \tilde{T}_\infty(\theta), \quad (\text{A6})$$

where $\tilde{T}_\infty(\theta)$ is determined by the matching condition with the bulk. The velocity can be obtained from the continuity equation (11) as

$$\tilde{u}(z, \theta) = \frac{2}{3}A \left(W(\theta) - \int_0^\theta \frac{z}{2\sqrt{\pi Av^3}} \exp\left(-\frac{z^2}{4Av}\right) W(\theta - v)dv \right). \quad (\text{A7})$$

It is important to note here that the velocity tends to a nonzero value at the edge of the boundary layer which reflects the fluid expansion and induces a compression perturbation in the bulk.

Substituting Eqs. (A4) and (A6) into the equation of state (15), the homogeneous character of the pressure in the boundary layer is expressed as

$$\tilde{P}(z, \theta) \equiv \bar{P}(\theta) = \frac{3}{2}\tilde{T}_\infty(\theta). \quad (\text{A8})$$

2. Bulk

The solution to the set of Eqs. (30), (32), (34), and (27b) along with the impervious boundary condition at $x = 1$ can be obtained in a straightforward manner yielding $\bar{\rho}$, \bar{T} , \bar{u} , and \bar{P} , namely,

$$\bar{\rho}(x, \theta) = \frac{2}{3}A \int_0^\theta W(v)dv, \quad (\text{A9})$$

$$\bar{T}(x, \theta) = \frac{A}{(\rho C_v)_{\text{eq}}} \int_0^\theta W(v)dv, \quad (\text{A10})$$

$$\bar{u}(x, \theta) = \frac{2}{3}AW(\theta)(1-x), \quad (\text{A11})$$

$$\bar{P}(x, \theta) = \frac{3}{2}\bar{T}(x, \theta). \quad (\text{A12})$$

Matching the temperature between the TBL and the bulk immediately provides the expression of $\tilde{T}_\infty(\theta)$ involved in Eq. (A6), i.e., $\tilde{T}_\infty(\theta) = \frac{A}{(\rho C_v)_{\text{eq}}} \int_0^\theta W(\theta)d\theta$.

3. Uniformly valid solutions ($0 \leq x \leq 1$)

When $\tau \gg \tau_{c1} = 1/\text{Re}_p^{4/3}$, uniformly valid solutions for $0 \leq x \leq 1$ are hence

$$\rho(x, \theta) = \frac{2}{3}A\tau^{1/2}\varphi \int_0^\theta \left(\tau W(v) - K_\rho\left(\frac{x}{\tau}, v\right)W(\theta-v) \right)dv, \quad (\text{A13})$$

$$T(x, \theta) = \varphi\tau^{3/2}A \left(\int_0^\theta K_\rho\left(\frac{x}{\tau}, v\right)W(\theta-v)dv + \frac{1}{(\rho C_v)_{\text{eq}}} \int_0^\theta W(v)dv \right), \quad (\text{A14})$$

$$u(x, \theta) = \frac{2}{3} \frac{A\varphi}{\text{Re}_a} \left(W(\theta)(1-x) - \int_0^\theta \frac{x}{2\tau\sqrt{\pi Av^3}} \exp\left(-\frac{x^2}{4\tau^2 Av}\right)W(\theta-v)dv \right), \quad (\text{A15})$$

$$P(x, \theta) = \frac{3}{2}\varphi\tau^{3/2} \frac{A}{(\rho C_v)_{\text{eq}}} \int_0^\theta W(v)dv, \quad (\text{A16})$$

where $K_\rho\left(\frac{x}{\tau}, v\right)$ is given by Eq. (A5).

APPENDIX B: SOLUTIONS AT THE FIRST CROSSOVER

This appendix reports on the balance equations for the TBL and the bulk, as well as the corresponding uniformly valid solutions for ρ , T , u , and p at the first crossover, i.e., when τ approaches $\tau_{c1} = 1/\text{Re}_p^{4/3}$ and for which the crossover parameter is $\tilde{\tau}_1 = \tau/\tau_{c1}$. Combining Eqs. (9) with orders of magnitude of Eq. (44) while using the TBL thickness $\delta = \tau_{c1}$ and timescale $\zeta = \text{Re}_a \text{Da}$, the following set of equations valid in the TBL is obtained:

$$\tilde{\rho}_\theta + \tilde{u}_z = 0, \quad (\text{B1})$$

$$\tilde{P}_z = 0, \quad (\text{B2})$$

$$0 = -\frac{3}{2}\tilde{u}_z + A\tilde{\tau}_1^{-1/2}\tilde{T}_{zz}, \quad (\text{B3})$$

$$\tilde{P} = \frac{3}{2}\tilde{T} + \frac{9}{4}\tilde{\tau}_1\tilde{\rho}, \quad (\text{B4})$$

$$\tilde{T}_z = -\tilde{\tau}_1^{1/2}W(\theta), \quad \text{at } z = 0, \theta \geq 0, \quad (\text{B5})$$

$$\tilde{\rho} = \tilde{u} = \tilde{T} = \tilde{P} = 0, \quad \text{at } \theta < 0, \quad (\text{B6})$$

$$\tilde{u}(z, \theta) = 0, \quad \text{at } z = 0. \quad (\text{B7})$$

In Eq. (B3), A is given by Eq. (A2),

Similarly, when Eqs. (27) are considered, the following conservation equations and boundary conditions valid in the bulk are obtained:

$$\bar{\rho}_\theta + \bar{u}_x = 0, \quad (\text{B8})$$

$$\bar{P}_x = -\gamma_0\bar{u}, \quad (\text{B9})$$

$$(\rho C_v)_{\text{eq}} \bar{T}_\theta = -\frac{3}{2} \bar{u}_x, \quad (\text{B10})$$

$$\bar{P} = \frac{3}{2} \bar{T}, \quad (\text{B11})$$

$$\bar{\rho} = \bar{u} = \bar{T} = \bar{P} = 0, \quad \text{at } \theta < 0, \quad (\text{B12})$$

$$\bar{u}(x, \theta) = 0, \quad \text{at } x = 1, \quad (\text{B13})$$

$$\bar{T}_x(x, \theta) = 0, \quad \text{at } x = 1. \quad (\text{B14})$$

These two sets of equations can be solved using the Laplace transform and when the matching conditions given by $\lim_{z \rightarrow \infty} \tilde{\eta}_\psi \tilde{\psi}(z, \theta) = \tilde{\eta}_\psi \tilde{\psi}(x = 0, \theta)$ ($\psi = (T, \rho, P, u)$) are applied, the following solutions, that are uniformly valid over space ($0 \leq x \leq 1$), are obtained. Density is given by

$$\rho(x, \theta) = -\frac{2}{3} A \tau_{c1}^{1/2} \varphi \int_0^\theta (K_{\rho 1}(x, v) - \tau_{c1} K_T(x, v)) W(\theta - v) dv, \quad (\text{B15})$$

where $K_{\rho 1}(v, x)$ is a Gaussian diffusion kernel defined as

$$K_{\rho 1}(x, v) = \frac{1}{\sqrt{\pi A_1(\tilde{\tau}_1) v}} \exp\left(-\frac{x^2}{4\tau_{c1}^2 A_1(\tilde{\tau}_1) v}\right), \quad (\text{B16})$$

in which $A_1(\tilde{\tau}_1) = A \tilde{\tau}_1^{1/2}$ and $K_T(x, v)$ is a kernel associated to the temperature,

$$K_T(x, v) = 1 + 2 \sum_{n=1}^{\infty} (-1)^n e^{-n^2 \pi^2 B v} \cos(n\pi(1-x)), \quad (\text{B17})$$

where

$$B = \frac{9}{4\gamma_0(\rho C_v)_{\text{eq}}}. \quad (\text{B18})$$

The solution for the temperature is

$$T(x, \theta) = A \tau_{c1}^{3/2} \varphi \int_0^\theta \left(\tau_1 K_{\rho 1}(x, v) + \frac{1}{(\rho C_v)_{\text{eq}}} K_T(x, v) \right) W(\theta - v) dv, \quad (\text{B19})$$

and the velocity is given by

$$u(x, \theta) = \frac{2}{3} \frac{A}{\text{Re}_a} \varphi \int_0^\theta \left(K_u(x, v) - \frac{x}{2\tau_{c1} \sqrt{\pi A_1(\tilde{\tau}_1) v^3}} \exp\left(-\frac{x^2}{4\tau_{c1}^2 A_1(\tilde{\tau}_1) v}\right) \right) W(\theta - v) dv. \quad (\text{B20})$$

In this last expression, $K_u(x, v)$ is the velocity kernel defined by

$$K_u(x, v) = 2\pi B \sum_{n=1}^{\infty} (-1)^{n+1} n e^{-n^2 \pi^2 B v} \sin(n\pi(1-x)), \quad x \neq 0, \quad K_u(0, v) = \delta(v), \quad (\text{B21})$$

in which $\delta(v)$ is the Dirac delta distribution at v .

Finally, the pressure is given by

$$p(x, \theta) = \frac{3}{2} \frac{A}{(\rho C_v)_{\text{eq}}} \tau_{c1}^{3/2} \varphi \int_0^\theta K_T(x, v) W(\theta - v) dv. \quad (\text{B22})$$

APPENDIX C: SOLUTIONS AT THE SECOND CROSSOVER

This appendix summarizes the results at the second crossover when τ is close to $\tau_{c2} = 1/\text{Re}_p^4$, the crossover parameter being defined as $\tilde{\tau}_2 = \tau/\tau_{c2}$. When orders of magnitude of Eq. (45) are introduced in the general balance equations [Eqs. (9)], keeping in mind that the TBL thickness and the timescale are respectively given by $\delta = \tau_{c2}^{1/2}$ and $\zeta = \text{Re}_a \text{Da}$, the following set of conservation equations and boundary conditions are obtained for the TBL:

$$\tilde{\rho}_\theta + \tilde{u}_z = 0, \quad (\text{C1})$$

$$\tilde{P}_z = -\gamma_0 \tilde{u}, \quad (\text{C2})$$

$$0 = -\frac{3}{2} \tilde{u}_z + A \tilde{\tau}_2^{-1/2} \tilde{T}_{zz}, \quad (\text{C3})$$

$$\tilde{P} = \frac{3}{2} \tilde{T} + \frac{9}{4} \tilde{\tau}_2 \tilde{\rho}, \quad (\text{C4})$$

$$\tilde{T}_z = -\tilde{\tau}_2^{1/2} W(\theta), \quad \text{at } z = 0, \theta \geq 0, \quad (\text{C5})$$

$$\tilde{\rho} = \tilde{u} = \tilde{T} = \tilde{P} = 0, \quad \text{at } \theta < 0, \quad (\text{C6})$$

$$\tilde{u}(z, \theta) = 0, \quad \text{at } z = 0, \quad (\text{C7})$$

where A is given by Eq. (A2).

Following the same procedure with Eqs. (27), one obtains the following equations valid in the bulk:

$$\bar{\rho}_\theta + \bar{u}_x = 0, \quad (\text{C8})$$

$$\bar{P}_x = -\gamma_0 \bar{u}, \quad (\text{C9})$$

$$(\rho C_v)_{\text{eq}} \bar{T}_\theta = -\frac{3}{2} \bar{u}_x, \quad (\text{C10})$$

$$\bar{P} = \frac{3}{2} \bar{T}, \quad (\text{C11})$$

$$\bar{\rho} = \bar{u} = \bar{T} = \bar{P} = 0, \quad \text{at } \theta < 0, \quad (\text{C12})$$

$$\bar{u}(x, \theta) = 0, \quad \text{at } x = 1, \quad (\text{C13})$$

$$\bar{T}_x(x, \theta) = 0, \quad \text{at } x = 1. \quad (\text{C14})$$

As for the first crossover, these two sets of equations can be solved using the Laplace transform along with the matching conditions given by $\lim_{z \rightarrow \infty} \tilde{\eta}_\psi \tilde{\psi}(z, \theta) = \bar{\eta}_\psi \bar{\psi}(x = 0, \theta)$ ($\psi = (T, \rho, P, u)$), yielding the following solutions for ρ , T , u , and p that are uniformly valid over space ($0 \leq x \leq 1$):

$$\rho(x, \theta) = \frac{2}{3} A_2(\tilde{\tau}_2) \tilde{\tau}_2^{-1/2} \varphi \int_0^\theta (-K_{\rho 2}(x, v) + \tau_{c2}^{1/2} K_T(x, v)) W(\theta - v) dv, \quad (\text{C15})$$

in which

$$A_2(\tilde{\tau}_2) = \frac{\tilde{\tau}_2}{A^{-1} \tilde{\tau}_2^{1/2} + \frac{4}{9} \gamma_0}, \quad (\text{C16})$$

and where $K_T(x, v)$ is given by Eq. (B17), whereas $K_{\rho_2}(x, v)$ is a Gaussian diffusion kernel defined as

$$K_{\rho_2}(x, v) = \frac{1}{\sqrt{\pi A_2(\tilde{\tau}_2)v}} \exp\left(-\frac{x^2}{4\tau_{c2}A_2(\tilde{\tau}_2)v}\right). \quad (\text{C17})$$

The solution for the temperature is

$$\begin{aligned} T(x, \theta) &= A_2(\tilde{\tau}_2)\tilde{\tau}_2^{-1/2}\tau_{c2}^{1/2}\varphi \int_0^\theta \left(\frac{1}{(\rho C_v)_{\text{eq}}} K_T(x, v) + \tau_{c2}^{1/2} \left(\tilde{\tau}_2 - \frac{4}{9}\gamma_0 A_2(\tilde{\tau}_2) \right) K_{\rho_2}(x, v) \right) W(\theta - v) dv, \end{aligned} \quad (\text{C18})$$

and for the velocity, it is given by

$$\begin{aligned} u(x, \theta) &= \frac{2}{3}A_2(\tilde{\tau}_2)\tilde{\tau}_2^{-1/2}\frac{1}{\text{Re}_a}\varphi \int_0^\theta \left(K_u(x, v) - \frac{x}{2\tau_{c2}^{1/2}\sqrt{\pi A_2(\tilde{\tau}_2)v^3}} \exp\left(-\frac{x^2}{4\tau_{c2}A_2(\tilde{\tau}_2)v}\right) \right) W(\theta - v) dv, \end{aligned} \quad (\text{C19})$$

where $K_u(x, v)$ is the velocity kernel given by Eq. (B21). The pressure is obtained as

$$p(x, \theta) = A_2(\tilde{\tau}_2)\tilde{\tau}_2^{-1/2}\tau_{c2}^{1/2}\varphi \int_0^\theta \left(\frac{3}{2(\rho C_v)_{\text{eq}}} K_T(x, v) - \frac{2}{3}\gamma_0\tau_{c2}^{1/2} K_{\rho_2}(x, v) \right) W(\theta - v) dv. \quad (\text{C20})$$

In this last expression, the term involving $K_{\rho_2}(x, v)$ has a negligible contribution since it is $\tau_{c2}^{1/2}$ times smaller than the term involving $K_T(x, v)$, whatever the value of $\tilde{\tau}_2$.

-
- [1] H. Stanley, *Introduction to Phase Transitions and Critical Phenomena* (Oxford University Press, New York, 1971).
 - [2] M. Moldover, J. Sengers, R. Gammon, and R. Hocken, Gravity effects in fluids near the gas-liquid critical point, *Rev. Mod. Phys.* **51**, 79 (1979).
 - [3] A. Onuki, H. Hao, and R. A. Ferrell, Fast adiabatic equilibration in a single-component fluid near the liquid-vapor critical point, *Phys. Rev. A* **41**, 2256 (1990).
 - [4] H. Boukari, J. N. Shaumeyer, M. E. Briggs, and R. W. Gammon, Critical speeding up in pure fluids, *Phys. Rev. A* **41**, 2260 (1990).
 - [5] B. Zappoli, D. Bailly, Y. Garrabos, B. Le Neindre, P. Guenoun, and D. Beysens, Anomalous heat transport by the piston effect in supercritical fluids under zero gravity, *Phys. Rev. A* **41**, 2264 (1990).
 - [6] P. Guenoun, B. Khalil, D. Beysens, Y. Garrabos, F. Kammoun, B. Le Neindre, and B. Zappoli, Thermal cycle around the critical point of carbon dioxide under reduced gravity, *Phys. Rev. E* **47**, 1531 (1993).
 - [7] M. Bonetti, F. Perrot, D. Beysens, and Y. Garrabos, Fast thermalization in supercritical fluids, *Phys. Rev. E* **49**, R4779 (1994).
 - [8] J. Straub, L. Eicher, and A. Haupt, Dynamic temperature propagation in a pure fluid near its critical point observed under microgravity during the German Spacelab Mission D-2, *Phys. Rev. E* **51**, 5556 (1995).
 - [9] Y. Garrabos, M. Bonetti, D. Beysens, F. Perrot, T. Fröhlich, P. Carlès, and B. Zappoli, Relaxation of a supercritical fluid after a heat pulse in the absence of gravity effects: Theory and experiments, *Phys. Rev. E* **57**, 5665 (1998).
 - [10] H. Boukari, M. E. Briggs, J. N. Shaumeyer, and R. W. Gammon, Critical speeding up observed, *Phys. Rev. Lett.* **65**, 2654 (1990).

-
- [11] A. Onuki and R. A. Ferrell, Adiabatic heating effect near the gas-liquid critical point, *Physica A* **164**, 245 (1990).
- [12] G. Accary and I. Raspo, A 3D finite volume method for the prediction of a supercritical fluid buoyant flow in a differentially heated cavity, *Comput. Fluids* **35**, 1316 (2006).
- [13] B. Zappoli, The response of a nearly supercritical pure fluid to a thermal disturbance, *Phys. Fluids A* **4**, 1040 (1992).
- [14] B. Zappoli and A. Durand-Daubin, Heat and mass transport in a near supercritical fluid, *Phys. Fluids* **6**, 1929 (1994).
- [15] B. Zappoli and P. Carles, The thermo-acoustic nature of the critical speeding up, *Eur. J. Mech. B/Fluids* **14**, 41 (1995).
- [16] D. Bailly and B. Zappoli, Hydrodynamic theory of density relaxation in near-critical fluids, *Phys. Rev. E* **62**, 2353 (2000).
- [17] B. Zappoli, Near-critical fluid hydrodynamics, *C. R. Mec.* **331**, 713 (2003).
- [18] M. Barmatz, I. Hahn, J. A. Lipa, and R. V. Duncan, Critical phenomena in microgravity: Past, present, and future, *Rev. Mod. Phys.* **79**, 1 (2007).
- [19] R. A. Wilkinson, G. A. Zimmerli, H. Hao, M. R. Moldover, R. F. Berg, W. L. Johnson, R. A. Ferrell, and R. W. Gammon, Equilibration near the liquid-vapor critical point in microgravity, *Phys. Rev. E* **57**, 436 (1998).
- [20] Y. Miura, S. Yoshihara, M. Ohnishi, K. Honda, M. Matsumoto, J. Kawai, M. Ishikawa, H. Kobayashi, and A. Onuki, High-speed observation of the piston effect near the gas-liquid critical point, *Phys. Rev. E* **74**, 010101(R) (2006).
- [21] A. Onuki, *Phase Transition Dynamics* (Cambridge University Press, Cambridge, 2002).
- [22] P. Carlès, The effect of bulk viscosity on temperature relaxation near the critical point, *Phys. Fluids* **10**, 2164 (1998).
- [23] P. Carlès and K. Dadzie, Two typical time scales of the piston effect, *Phys. Rev. E* **71**, 066310 (2005).
- [24] B. Zappoli and P. Carles, Acoustic saturation of the critical speeding up, *Physica D* **89**, 381 (1996).
- [25] Y. Chiwata and A. Onuki, Thermal plumes and convection in highly compressible fluids, *Phys. Rev. Lett.* **87**, 144301 (2001).
- [26] A. B. Kogan and H. Meyer, Heat transfer and convection onset in a compressible fluid: He near the critical point, *Phys. Rev. E* **63**, 056310 (2001).
- [27] J. Yoo, The turbulent flows of supercritical fluids with heat transfer, *Annu. Rev. Fluid Mech.* **45**, 495 (2013).
- [28] J. Ren, O. Marxen, and R. Pecnik, Boundary-layer stability of supercritical fluids in the vicinity of the Widom line, *J. Fluid Mech.* **871**, 831 (2019).
- [29] J. Robinet and X. Gloerfelt, Instabilities in non-ideal fluids, *J. Fluid Mech.* **880**, 1 (2019).
- [30] D. Beysens, D. Chatain, P. Evesque, and Y. Garrabos, High-frequency driven capillary flows speed up the gas-liquid phase transition in zero-gravity conditions, *Phys. Rev. Lett.* **95**, 034502 (2005).
- [31] D. Beysens, Vibrations in space as an artificial gravity? *Europhys. News* **37**, 22 (2006).
- [32] Y. Garrabos, D. Beysens, C. Lecoutre, A. Dejoan, V. Polezhaev, and V. Emelianov, Thermoconvective phenomena induced by vibrations in supercritical SF₆ under weightlessness, *Phys. Rev. E* **75**, 056317 (2007).
- [33] D. Beysens, Y. Garrabos, D. Chatain, and P. Evesque, Phase transition under forced vibrations in critical CO₂, *Europhys. Lett.* **86**, 16003 (2009).
- [34] L. Chen, R. Zhang, Y. Kanda, D. Basu, A. Komiya, and H. Chen, Asymptotic analysis of boundary thermal-wave process near the liquid-gas critical point, *Phys. Fluids* **34**, 036102 (2022).
- [35] R. Zhang, J. Xu, and L. Chen, Asymptotic thermophysical behaviors of near-critical fluid under parameter scaling, *Int. J. Heat Fluid Flow* **108**, 109442 (2024).
- [36] D. Yu, K. Jackson, and T. Harmon, Dispersion and diffusion in porous media under supercritical conditions, *Chem. Eng. Sci.* **54**, 357 (1999).
- [37] B. Shannon, W. Hendrix, B. Smith, and G. Motero, Modeling of supercritical fluid flow through a yarn package, *J. Supercrit. Fluids* **19**, 87 (2000).

- [38] F. Cansell, C. Aymonier, and A. Loppinet-Serani, Review of materials science and supercritical fluids, [Curr. Opin. Solid State Mater. Sci.](#) **7**, 331 (2003).
- [39] C. A. García-González, A. Concheiro, and C. Alvarez-Lorenzo, Instabilities in non-ideal fluids, [Bioconjugate Chem.](#) **26**, 1159 (2015).
- [40] C. Doughty and K. Pruess, Modeling supercritical carbon dioxide injection in heterogeneous porous media, [Vadose Zone J.](#) **3**, 837 (2004).
- [41] N. Henderson, E. Flores, M. Sampaio, L. Freitas, and G. Platt, Supercritical fluid flow in porous media: modeling and simulation, [Chem. Eng. Sci.](#) **60**, 1797 (2005).
- [42] K. Sasaki, T. Fujii, Y. Niibori, T. Ito, and T. Hashida, Numerical simulation of supercritical CO₂ injection into subsurface rock masses, [Energy Convers. Manage.](#) **49**, 54 (2008).
- [43] E. Soboleva, Effects of strong compressibility in natural convective flows through porous media with a near-critical fluid, [Fluid Dyn.](#) **43**, 217 (2008).
- [44] M. Chen and L. Chen, Numerical study of CO₂ trans-critical process inside micromodel based porous structures under supercritical pressures, [Int. J. Heat Fluid Flow](#) **107**, 109361 (2024).
- [45] M. Skuntz, J. Seymour, and R. Anderson, Observation of heat transfer due to variable thermophysical properties of sub-, near- and super- critical fluids in porous media by magnetic resonance imaging, [Int. Commun. Heat Mass Transfer](#) **128**, 105635 (2021).
- [46] R. Zhang and L. Chen, Asymptotic analysis of fluid thermodynamic behaviors in the near-critical region under highly variable physical properties, [Heat Transfer Eng.](#) (2024), doi:10.1080/01457632.2024.2368431.
- [47] A. Altevogt, D. Rolston, and S. Whitaker, New equations for binary gas transport in porous media, part 1: Equation development, [Adv. Water Resour.](#) **26**, 695 (2003).
- [48] D. Lasseux, F. Valdés-Parada, and F. Bellet, Macroscopic model for unsteady flow in porous media, [J. Fluid Mech.](#) **862**, 283 (2019).
- [49] S. Whitaker, *The Method of Volume Averaging* (Springer Netherlands, Dordrecht, 1999).
- [50] S. Whitaker, The Forchheimer equation: A theoretical development, [Transp. Porous Med.](#) **25**, 27 (1996).
- [51] D. Lasseux, A. A. Abbasian Arani, and A. Ahmadi, On the stationary macroscopic inertial effects for one phase flow in ordered and disordered porous media, [Phys. Fluids](#) **23**, 073103 (2011).
- [52] M. Quintard and S. Whitaker, Local thermal equilibrium for transient heat conduction: Theory and comparison with numerical experiments, [Int. J. Heat Mass Transf.](#) **38**, 2779 (1995).
- [53] J. Maxwell, *A Treatise on Electricity and Magnetism, Vol. 1* (Clarendon Press, Oxford, 1891, reprinted by Dover, New York, 1954).